High Mg activation in implanted GaN by high temperature and ultrahigh pressure annealing

Cite as: Appl. Phys. Lett. 118, 022101 (2021); https://doi.org/10.1063/5.0038628 Submitted: 24 November 2020 . Accepted: 24 December 2020 . Published Online: 12 January 2021

D M. Hayden Breckenridge, James Tweedie, D Pramod Reddy, Yan Guan, D Pegah Bagheri, D Dennis Szymanski, Seiji Mita, Kacper Sierakowski, Michał Boćkowski, Ramon Collazo, and D Zlatko Sitar







ARTICLES YOU MAY BE INTERESTED IN

Vertical p-type GaN Schottky barrier diodes with nearly ideal thermionic emission characteristics

Applied Physics Letters 118, 022102 (2021); https://doi.org/10.1063/5.0036093

Progress on and challenges of p-type formation for GaN power devices

Journal of Applied Physics 128, 090901 (2020); https://doi.org/10.1063/5.0022198

Nitrogen-displacement-related electron traps in n-type GaN grown on a GaN freestanding substrate

Applied Physics Letters 118, 012106 (2021); https://doi.org/10.1063/5.0035235





High Mg activation in implanted GaN by high temperature and ultrahigh pressure annealing

Cite as: Appl. Phys. Lett. **118**, 022101 (2021); doi: 10.1063/5.0038628 Submitted: 24 November 2020 · Accepted: 24 December 2020 · Published Online: 12 January 2021







M. Hayden Breckenridge,^{1,a)} D James Tweedie,² Pramod Reddy,² D Yan Guan,¹ Pegah Bagheri,¹ D Dennis Szymanski,¹ Seiji Mita,² Kacper Sierakowski,³ Michał Boćkowski,³ Ramon Collazo,¹ and Zlatko Sitar^{1,2} D

AFFILIATIONS

Department of Materials Science and Engineering, North Carolina State University, Raleigh, North Carolina 27695-7919, USA

ABSTRACT

We demonstrate high p-type conductivity and hole concentrations $>10^{18}$ cm⁻³ in Mg-implanted GaN. The implantation was performed at room temperature and by post-implantation annealing at 1 GPa of N₂ and in a temperature range of $1200-1400\,^{\circ}$ C. The high pressure thermodynamically stabilized the GaN surface without the need of a capping layer. We introduce a "diffusion budget," related to the diffusion length, as a convenient engineering parameter for comparing samples annealed at different temperatures and for different times. Although damage recovery, as measured by XRD, was achieved at relatively low diffusion budgets, these samples did not show p-type conductivity. Further analyses showed heavy compensation by the implantation-induced defects. Higher diffusion budgets resulted in a low Mg ionization energy (\sim 115 meV) and almost complete Mg activation. For even higher diffusion budgets, we observed significant loss of Mg to the surface and a commensurate reduction in the hole conductivity. High compensation at low diffusion budgets and loss of Mg at high diffusion budgets present a unique challenge for shallow implants. A direct control of the formation of compensating defects arising from the implantation damage may be necessary to achieve both hole conductivity and low Mg diffusion.

Published under license by AIP Publishing. https://doi.org/10.1063/5.0038628

GaN-based high-power switches are a promising avenue toward realizing low-loss power grids.^{1,2} Reduced power losses and higher currents leading to higher efficiencies are expected in devices such as vertical GaN current aperture vertical electron transistor (CAVET) and junction field effect transistor (JFET) power switches.3-Controlling the selective area doping of both n- and p-regions is necessary to realize these device structures. Although controlled p-type carrier concentrations and conductivities in GaN have been reproducibly demonstrated by Mg doping during epitaxy, achieving p-type conductivity with selective area doping remains a challenge. Mg diffusion studies into unintentionally doped GaN films have been attempted with only limited success. Issues of high thermal diffusion temperatures, degradation of the GaN surface, and a nonuniform Mg doping profile have inhibited the adoption of this technique for selective area p-doping in GaN.⁶⁻⁸ The technique of choice for selective area doping in Si- and SiC-based technology is ion implantation. 9,10 Despite early success in n-type doping of GaN via ion implantation, 11 p-type doping via ion implantation in III-nitrides remains a challenge. The primary challenge lies in GaN being thermodynamically unstable for T > 850 °C as ion implantation introduces significant lattice distortion that is typically removed via a high temperature post-implantation anneal (T \geq 1200 °C). In order to prevent surface decomposition during annealing at these elevated temperatures, previous effort has focused on the use of capping layers (e.g., AlN, Si₃N₄, and SiO₂) and/ or complex annealing procedures. However, several challenges exist including the introduction of impurities, alloying, and etch damage in p-GaN during capping layer removal. 12,13 In this work, we demonstrate p-type conductivity in GaN films via room temperature Mg implantation and a post-implantation anneal at a high pressure (1 GPa) that stabilized the GaN surface without the use of a capping layer. Recent work by Sakurai et al. has shown the effectiveness of annealing at high pressure at a temperature of 1400 °C with a dwell time of 5 min.¹⁴ In the present study, we have explored a series of annealing temperatures and times to develop a model for Mg activation in GaN in terms of a diffusion budget (DB) that enables prediction of hole sheet conductivity. These studies show the effects of

²Adroit Materials, Inc., 2054 Kildaire Farm Rd., Cary, North Carolina 27518, USA

³Institute of High-Pressure Physics, Polish Academy of Sciences, Sokołowska 29/37, 01-142 Warsaw, Poland

a) Author to whom correspondence should be addressed: mhbrecke@ncsu.edu

annealing temperature and time, summarized in terms of a diffusion budget, describing the correlation between the crystal lattice damage recovery, dopant activation, dopant diffusion, and self-compensation. Finally, we demonstrate a technologically relevant room temperature p-type sheet carrier concentration greater than 10^{13} cm $^{-2}$ via Mg ion implantation and high-pressure annealing (1 GPa) at temperatures between $1200\,^{\circ}$ C and $1400\,^{\circ}$ C.

1.5'' semi-insulating GaN wafers grown by the ammonothermal method from IHPP PAS (formerly Ammono, S. A.) were used for these studies. These wafers were compensated with Mn and had a resistivity $\geq\!10^9~\Omega$ cm. They were free of macro-defects and had an etch pit density (EPD) $<\!5\times10^4~cm^{-2}$. The FWHM of the (0 0 0 2) x-ray rocking curve was $\sim\!20~arc$ sec, indicating a dislocation density on the order of $10^4~cm^{-2}$.

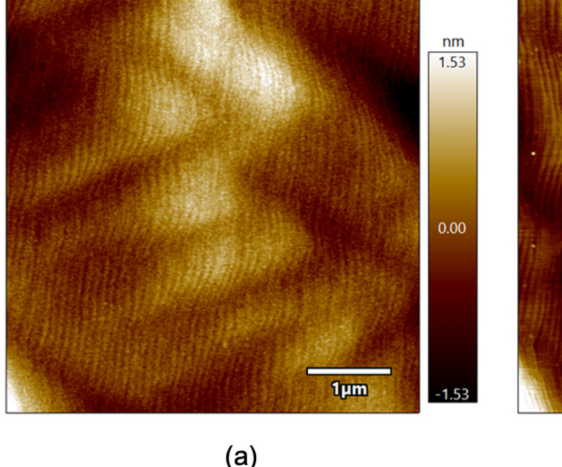
Unintentionally doped homoepitaxial GaN films (\sim 2.5 μ m) were grown by metal organic chemical vapor deposition (MOCVD) on these wafers and then implanted with Mg⁺ ions. The implantation parameters were determined via Stopping and Range of Ions in Matter (SRIM)-Transport of Ions in Matter (TRIM) simulations in order to achieve a shallow box profile (~50 nm) of implanted Mg at a technologically relevant concentration of $\sim 2 \times 10^{19}$ cm⁻³. To realize the targeted Mg profile, a two-step implantation process that included ion energies of 50 and 20 keV with corresponding ion dosages of 1.0×10^{14} and 4.0×10^{13} cm⁻² was used, respectively. All implantations were performed at room temperature with a tilt angle of 7°. Mg and other impurity concentrations (C, O, Si, and H) were characterized by secondary ion mass spectroscopy (SIMS). Surface morphology before and after annealing was analyzed using an Asylum Research MFP-3D atomic force microscope (AFM). The ultrahigh pressure annealing (UHPA) procedure was performed at \sim 1 GPa using a nitrogen (5N) atmosphere, where GaN is stable up to a temperature of \sim 1500 °C. 15-17 Ultrahigh N₂ pressure during the annealing process thermodynamically stabilizes the GaN surface, which would, otherwise, decompose at these annealing temperatures. During the activation anneals, the samples were held at the annealing temperature $(700 \,^{\circ}\text{C}-1400 \,^{\circ}\text{C})$ for 10 or 100 min. The ramp-up time was \sim 20 min, and the ramp-down time to \sim 700 $^{\circ}$ C was on the order of minutes.

Implantation damage and post-annealing recovery of crystallinity were characterized by x-ray diffraction using a PANalytical X'Pert MRD to record ω -2 θ scans of symmetric reflections. The sheet concentration, mobility, and carrier type were determined using an 8400 series LakeShore AC/DC Hall measurement system. The AC Hall measurements were performed using a magnetic field and excitation field frequency of \sim 0.62 T and 100 mHz, respectively. The sheet carrier concentration and mobility were measured as a function of temperature in the temperature range of 300–773 K.

No surface degradation was observed on the annealed samples as observed under AFM (Fig. 1), even though no capping layer was employed to stabilize the surface. The surface of the homoepitaxial GaN films had a smooth bilayer step structure (RMS ≤ 1 nm) both asgrown (not shown) and after implantation [Fig. 1(a)]. Even at the maximum annealing temperature of $1400\,^{\circ}\text{C}$, the bilayer step surface was preserved [Fig. 1(b)]. There was no evidence of decomposition. Hence, at all annealing temperatures $\leq 1400\,^{\circ}\text{C}$, the 1 GPa N₂ pressure was sufficient to stabilize the surface.

Mg implantation damage is assumed to consist of displaced Ga and N matrix atoms from their lattice sites due to momentum transfer during implantation. The damage manifests itself as a significant strain profile in the implantation direction. After implantation, a series of XRD peaks appeared at low angles in the ω -2 θ profile of the symmetric (0 0 0 2) reflection (Fig. 2). These peaks corresponded to the strain profile of the implanted region. 19 It is standard practice to anneal the samples after implantation in order to recover crystallinity, reduce implantation damage associated with point and extended defects, and eliminate the resulting strain. 19,20 Keeping the annealing time at 10 min, with increasing annealing temperature, there was a significant reduction in the intensity of the strain-related peaks, indicating a corresponding reduction of the implantation-induced damage, as shown in Fig. 2. It is clear that a majority of strain relief occurred by annealing at 1200 °C. After increasing the annealing time to 100 min, or annealing at 1300 °C for 10 min, recovery of the crystal lattice damage was achieved, as demonstrated by XRD.

Further, the influence of annealing on the implanted Mg profile was investigated by secondary ion mass spectroscopy (SIMS) (with an



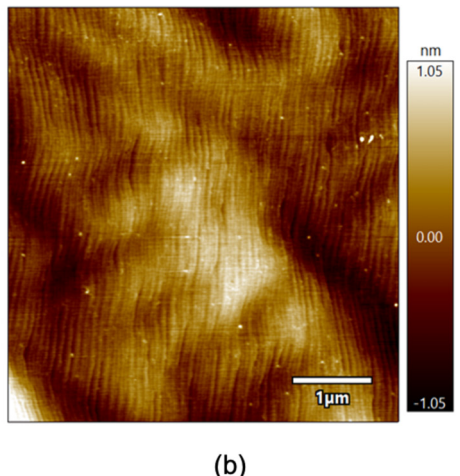


FIG. 1. AFM scans of (a) as-implanted homoepitaxial GaN film and (b) GaN surface after annealing at 1400 °C and 1 GPa N₂, for 10 min.

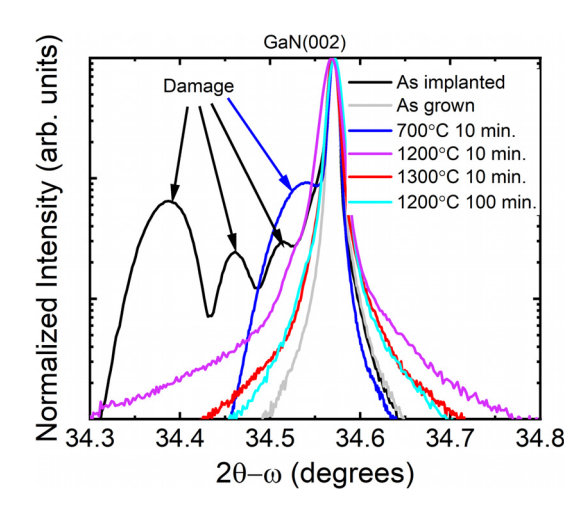


FIG. 2. XRD ω -2 θ profiles for a series of Mg-Implanted and annealed homoepitaxial GaN films.

Mg detection background of $<10^{16} \,\mathrm{cm}^{-3}$) in the as-implanted condition and after the activation anneals at various temperatures and for different times, as shown in Fig. 3. The as-implanted Mg profile is characterized by a peak Mg concentration of $\sim 2 \times 10^{19} \text{ cm}^{-3}$ with a range of \sim 40 nm to \sim 25 nm of longitudinal straggle, consistent with the TRIM simulations. No observable bulk diffusion occurred at 1200 °C and 10 min. Annealing for higher temperatures and times clearly resulted in bulk diffusion as evidenced by broadening of the Gaussian profile with a decrease in the peak dopant concentration. The peak Mg concentration was reduced to $<2 \times 10^{18} \text{ cm}^{-3}$ after annealing at 1300 °C for 100 min, and a significant Mg concentration $(>7 \times 10^{17} \text{ cm}^{-3})$ was observed at depths >400 nm. The XRD and SIMS analyses demonstrated a clear contrast between crystal damage recovery occurring for temperatures ≤1200 °C at 10 min and the bulk diffusion occurring at higher annealing temperatures and longer annealing times. This indicated that the mechanism of damage recovery was related to a fast and short-range diffusion with a lower activation energy that occurred before the onset of bulk diffusion.

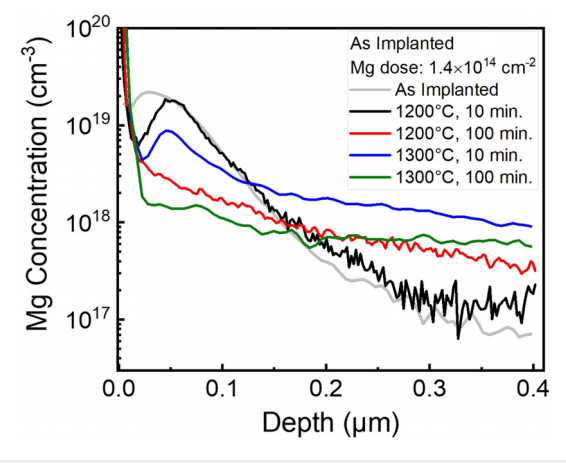


FIG. 3. SIMS profile of Mg-implanted GaN films before and after a series of anneals at 1 GPa of N_2 .

The p-type conductivity of the implanted region is a function of Mg activation, i.e., the concentration of substitutional Mg_{Ga} (N_A) and total compensation, N_D. Accordingly, to understand the influence of the short-range diffusion associated with damage recovery and bulk diffusion on the formation of MgGa and compensation, and hence p-type conductivity, temperature-dependent AC Hall measurements were performed for all samples. Interestingly, at 1200 °C and 10 min, where damage recovery was observed via XRD but no significant bulk diffusion of Mg was observed via SIMS, the samples were highly resistive, indicating either low Mg activation (unlikely) or high compensation in the implanted region. In contrast, all samples annealed at higher temperatures or for longer times showed p-type conductivity with high Mg activation, as shown in Fig. 4. All these samples also showed different degrees of bulk diffusion of Mg, as shown in Fig. 3. Using the SIMS data from Fig. 3, the Mg content after annealing is reported in Table I. These values were obtained by taking the integral of each SIMS curve and dividing the value by the initial Mg dose of 1.4×10^{14} cm⁻². By estimating the effective Mg doping thickness to be \sim 1 μ m (determined by SIMS), the maximum bulk hole concentration and hole mobility for the sample annealed at 1300 °C for 100 min measured by AC Hall at room temperature were $\sim 1.1 \times 10^{18} \, \text{cm}^{-3}$ and \sim 18 cm²/V s, respectively, demonstrating the capability of achieving technologically important hole concentrations via Mg implantation in GaN by high-temperature and high-pressure annealing.

In contrast to the present GaN study, previous work has shown that annealing of Mg-implanted GaAs achieved Mg activation and p-type conductivity without significant bulk diffusion, indicating that the fast, short-range diffusion associated with damage recovery was sufficient to produce the MgGa acceptor configuration without significant compensation.^{21,22} Further, increasing the annealing times in GaAs resulted in both bulk diffusion and increased resistivity. This resistivity increase was attributed to Mg diffusion to the surface and compensation.²¹ This is contrary to our observations in Mg:GaN, which shows strong compensation upon initial damage recovery and p-type conductivity only upon long-range diffusion of Mg atoms. At the moment, it is not clear if there is a significant difference in the p-type conductivities of the implanted and diffused regions upon high-temperature annealing. Within a single layer model, we can define an effective Mg activation ratio as the ratio between the maximum observed carrier concentration, i.e., (N_A-N_D) measured at high temperature, where all activated but not compensated acceptors produce free holes, and the Mg implanted dose, as a figure of merit. Although this is an established practice in characterization of semiconductors, one needs to be aware that this method lumps together two effects: (1) the actual Mg activation or positioning of the dopant on the desired lattice site and (2) compensation by a donor point defect, which can be extrinsic or intrinsic.

Further, we study the effective Mg activation ratio as a function of Mg bulk diffusion, which is characterized by the diffusion length,

$$L_D = 2\sqrt{Dt},\tag{1}$$

where t is the annealing time and D is the diffusion constant for Mg in GaN at a given temperature. Since the diffusion constant depends greatly on the sample condition (extended and point defects), the calculated L_D may significantly deviate from measurements. While L_D can be directly measured by SIMS, the process is time consuming and can produce significant error in the concentration and depth.

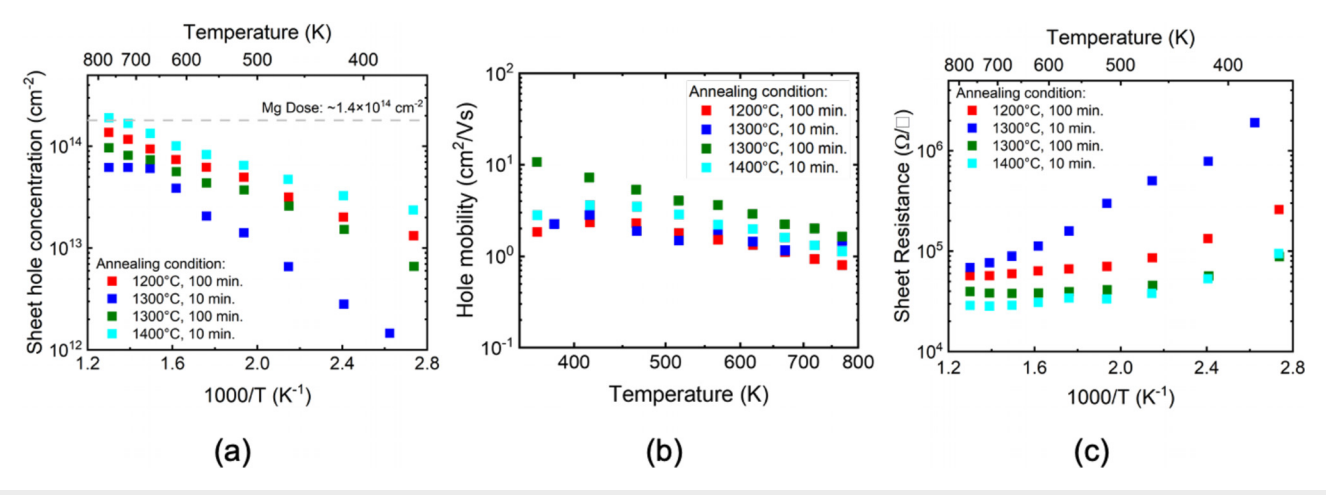


FIG. 4. (a) Sheet hole concentration, (b) hole mobility, and (c) sheet resistance of Mg-implanted homoepitaxial GaN as a function of temperature.

Since both the diffusion constant and the bandgap are a function of the bond strength, we introduce the diffusion budget, DB(T, t), in the form of

$$DB = Ae^{-T_0/T}t, (2)$$

where $T_0 = E_g/2k$, E_g is the material bandgap, k is the Boltzmann constant, and A is a scaling parameter chosen to be 2 s⁻¹. As defined, DB(T,t) becomes a convenient engineering parameter for comparison of samples annealed at different temperatures and for different times, which is related to the diffusion length. Table I summarizes annealing conditions, DB(T,t), and sheet carrier concentrations for various samples. A general trend evident in this table is that a certain DB budget is needed to achieve p-type conductivity. However, when the dependence of the sheet hole concentration and % of active Mg, $(N_A-N_D)/[Mg]$, on DB is plotted in Fig. 5(a), one can see that the hole concentration reaches a maximum and drops off for lower and higher diffusion budgets.

As discussed earlier, the sharp drop in the effective Mg activation at very low diffusion budgets is due to compensation within the implanted region. The source of compensation is implantation damage-related defects such as $V_{\rm N}$ or related complexes. At higher diffusion budgets, the gradual decrease in effective Mg activation is likely due to Mg segregating at the surface, as also observed in GaAs, i.e., a net reduction of the Mg concentration in the bulk GaN, as evident

from the decreasing Mg content obtained from the SIMS data in Fig. 3 and reported in Table $\rm L^{21}$

To further verify our hypothesis that lowered effective Mg activation is a consequence of compensation, we analyzed the temperature dependence of the hole concentration based on the charge neutrality expression given by

$$\frac{p(p+N_D)}{N_A-N_D-p} = \frac{N_V}{g} \exp\left(-\frac{E_i}{k_B T}\right),\tag{3}$$

where p is the hole concentration, N_D is the compensation by donors, N_A is the $\mathrm{Mg_{Ga}}$ concentration, T is the temperature, N_V is the effective density of states in the valence band, and E_i is the acceptor level measured with respect to the valence band, i.e., the ionization energy of Mg. From Eq. (3), it is clear that for samples with high compensation $(p \ll N_D)$,

$$\ln\left(p\right) \propto -\frac{E_i}{kT}.\tag{4}$$

Hence, the apparent carrier ionization energy E_{app} obtained from the semi-log plot of carrier concentration p as a function of 1/T becomes $E_{app} \sim E_i$. In contrast, for samples with low compensation $(p \gg N_D)$,

$$p^2 \propto \exp\left(-\frac{E_i}{kT}\right),$$
 (5)

TABLE I. Annealing conditions, maximum sheet hole concentrations, apparent ionization energies, and Mg content after annealing for various diffusion budgets, DBs.

| Diffusion budget | Anneal T (°C) | Anneal t (min) | Max. sheet hole conc. (cm ⁻²) | Apparent ionization energy (meV) | $[Mg]/(1.4 \times 10^{14} \text{ cm}^{-2})$ (%) |
|---------------------|---------------|----------------|---|----------------------------------|---|
| 0.04 | 1200 | 10 | | | >90 |
| 0.12 | 1300 | 10 | 6.5×10^{13} | 277 | >90 |
| 0.24 | 1400 | 10 | 1.4×10^{14} | 117 | |
| 0.44 | 1200 | 100 | 1.2×10^{14} | 137 | ${\sim}80$ |
| 1.10 | 1300 | 100 | 1.0×10^{14} | 160 | ~60 |

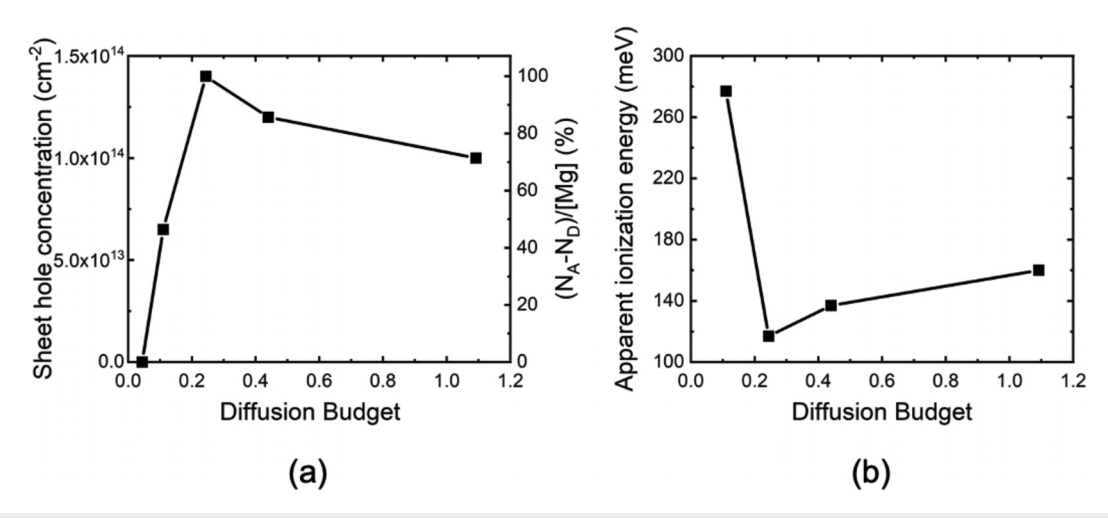


FIG. 5. The dependence of (a) maximum hole concentration and $(N_A - N_D) / [Mg]$ and (b) apparent activation energy on the diffusion budget.

and hence,

$$\ln\left(p\right) \propto -\frac{E_i}{2kT}.$$
(6)

Hence, the apparent carrier ionization energy E_{app} obtained from the semi-log plot of carrier concentration p as a function of 1/T becomes $E_{app} \sim E_i/2$. Therefore, from Eqs. (4) and (6), we expect a higher apparent carrier ionization energy for samples with higher compensation. The dependence of the apparent carrier ionization energy, E_{app} , as a function of diffusion budget is shown in Fig. 5(b). From the correlation of the change in E_{app} and the effective Mg activation ratio, it is clear that compensation is the primary cause of low effective Mg activation ratios in samples annealed with low diffusion budgets. Accordingly, E_{app} decreased from 280 meV for samples annealed at 1300 °C for 10 min to 115 meV for samples annealed at 1400 °C for 10 min. Hence, we conclude that, while Mg may be activated at lower diffusion budgets (1200 °C for 10 min), i.e., reside on the Ga site, the compensation is very high, likely due to point defects associated with implantation damage. Reducing the point defects is necessary and requires an increase in the diffusion budget. Interestingly, increasing the diffusion budget beyond an optimal value also results in an increase in E_{app} , as shown in Fig. 5(b). This may be explained by the reduction in N_A due to surface accumulation of Mg, resulting in an increased compensation ratio N_D/N_A and, hence, an increase in E_{app} .

While larger diffusion budgets are necessary for reducing compensation and an increased effective Mg activation, it is important to note that arbitrarily increasing the diffusion budget presents challenges in achieving shallow Mg implants due to the loss of Mg to the surface. As such, direct control of the formation of compensating defects arising from the implantation damage is necessary to achieve Mg activation during short-range diffusion, where surface accumulation is insignificant. Several point defect control techniques such as defect quasi Fermi level control and co-implantation may need to be implemented to produce shallow active Mg implants. ^{23–26}

We have demonstrated p-type conductivity in Mg-implanted GaN. Post-implantation annealing at high N₂ pressures (1 GPa)

thermodynamically stabilized the GaN surface without the need of a capping layer. We introduced diffusion budget as a convenient engineering parameter for comparing samples annealed at different temperatures and for different times. While damage recovery, as measured by XRD strain, was achieved at relatively low diffusion budgets, these samples remained insulating due to high compensation by the implantation-induced defects. Higher diffusion budgets produced sheet hole concentrations exceeding $10^{14}\,\mathrm{cm}^{-2}$, at an ionization energy as low as 115 meV and an Mg activation as high as \sim 100%. For high diffusion budgets, we observed significant Mg loss to the surface and commensurate reduction in the hole conductivity. Direct control of the formation of compensating defects arising from the implantation damage is necessary to achieve hole conductivity in Mg-implanted GaN and control the diffusion length.

The authors gratefully acknowledge funding in part from DOE (No. DE-AR0000873), AFOSR (Nos. FA-95501710225 and FA9550-1910114), NSF (Nos. ECCS-1916800 and ECCS-1653383), and Polish National Science Centre (No. 2018/29/B/ST5/00338).

DATA AVAILABILITY

The data that support the findings of this study are available within the article.

REFERENCES

¹H. Amano, Y. Baines, E. Beam, M. Borga, T. Bouchet, P. R. Chalker, M. Charles, K. J. Chen, N. Chowdhury, R. Chu, C. D. Santi, M. M. D. Souza, S. Decoutere, L. D. Cioccio, B. Eckardt, T. Egawa, P. Fay, J. J. Freedsman, L. Guido, O. Häberlen, G. Haynes, T. Heckel, D. Hemakumara, P. Houston, J. Hu, M. Hua, Q. Huang, A. Huang, S. Jiang, H. Kawai, D. Kinzer, M. Kuball, A. Kumar, K. B. Lee, X. Li, D. Marcon, M. März, R. McCarthy, G. Meneghesso, M. Meneghini, E. Morvan, A. Nakajima, E. M. S. Narayanan, S. Oliver, T. Palacios, D. Piedra, M. Plissonnier, R. Reddy, M. Sun, I. Thayne, A. Torres, N. Trivellin, V. Unni, M. J. Uren, M. V. Hove, D. J. Wallis, J. Wang, J. Xie, S. Yagi, S. Yang, C. Youtsey, R. Yu, E. Zanoni, S. Zeltner, and Y. Zhang, J. Phys. Appl. Phys. 51, 163001 (2018).

²J. Y. Tsao, S. Chowdhury, M. A. Hollis, D. Jena, N. M. Johnson, K. A. Jones, R. J. Kaplar, S. Rajan, C. G. Van de Walle, E. Bellotti, C. L. Chua, R. Collazo, M.

- E. Coltrin, J. A. Cooper, K. R. Evans, S. Graham, T. A. Grotjohn, E. R. Heller, M. Higashiwaki, M. S. Islam, P. W. Juodawlkis, M. A. Khan, A. D. Koehler, J. H. Leach, U. K. Mishra, R. J. Nemanich, R. C. N. Pilawa-Podgurski, J. B. Shealy, Z. Sitar, M. J. Tadjer, A. F. Witulski, M. Wraback, and J. A. Simmons, Adv. Electron. Mater. 4, 1600501 (2018).
- ³S. Chowdhury, M. H. Wong, B. L. Swenson, and U. K. Mishra, IEEE Electron Device Lett. **33**, 41 (2012).
- ⁴D. Ji, Y. Yue, J. Gao, and S. Chowdhury, IEEE Trans. Electron Devices 63, 4011 (2016).
- ⁵D. Ji and S. Chowdhury, IEEE Trans. Electron Devices **62**, 3633 (2015).
- ⁶C. J. Pan and G. C. Chi, Solid-State Electron. **43**, 621 (1999).
- ⁷G. C. Chi, C. H. Kuo, J. K. Sheu, and C. J. Pan, Mater. Sci. Eng. B 75, 210 (2000).
- ⁸Y.-J. Yang, J.-L. Yen, F.-S. Yang, and C.-Y. Lin, Jpn. J. Appl. Phys., Part 2 39, L390 (2000).
- ⁹L. Rubin and J. Poate, Ind. Phys. **9**, 12 (2003).
- ¹⁰V. Heera, D. Panknin, and W. Skorupa, Appl. Surf. Sci. 184, 307 (2001).
- ¹¹J. K. Sheu, C. J. Tun, M. S. Tsai, C. C. Lee, G. C. Chi, S. J. Chang, and Y. K. Su, J. Appl. Phys. **91**, 1845 (2002).
- ¹²W. Khalfaoui, T. Oheix, G. El-Zammar, R. Benoit, F. Cayrel, E. Faulques, F. Massuyeau, A. Yvon, E. Collard, and D. Alquier, Phys. Status Solidi A 214, 1600438 (2017).
- ¹³K. Fu, H. Fu, H. Liu, S. R. Alugubelli, T.-H. Yang, X. Huang, H. Chen, I. Baranowski, J. Montes, F. A. Ponce, and Y. Zhao, Appl. Phys. Lett. 113, 233502 (2018).
- ¹⁴ H. Sakurai, M. Omori, S. Yamada, Y. Furukawa, H. Suzuki, T. Narita, K. Kataoka, M. Horita, M. Bockowski, J. Suda, and T. Kachi, Appl. Phys. Lett. 115, 142104 (2019).

- ¹⁵K. T. Jacob and G. Rajitha, J. Cryst. Growth **311**, 3806 (2009).
- ¹⁶S. Porowski, I. Grzegory, D. Kolesnikov, W. Lojkowski, V. Jager, W. Jager, V. Bogdanov, T. Suski, and S. Krukowski, J. Phys. 14, 11097 (2002).
- ¹⁷K. Sierakowski, R. Jakiela, B. Lucznik, P. Kwiatkowski, M. Iwinska, M. Turek, H. Sakurai, T. Kachi, and M. Bockowski, Electronics 9, 1380 (2020).
- ¹⁸K. Hogan, S. Tozier, E. Rocco, I. Mahaboob, V. Meyers, B. McEwen, F. Shahedipour-Sandvik, R. Tompkins, M. Derenge, K. Jones, M. Shevelev, V. Sklyar, A. Lang, J. Hart, M. Taheri, and M. Reshchikov, in 2019 IEEE International Reliability Physics Symposium (IRPS) (2019), pp. 1–6.
- ¹⁹Y. Wang, K. Huynh, M. E. Liao, H.-M. Yu, T. Bai, J. Tweedie, M. H. Breckenridge, R. Collazo, Z. Sitar, M. Bockowski, Y. Liu, and M. S. Goorsky, Phys. Status Solidi B 257, 1900705 (2020).
- ²⁰K. Iwata, H. Sakurai, S. Arai, T. Nakashima, T. Narita, K. Kataoka, M. Bockowski, M. Nagao, J. Suda, T. Kachi, and N. Ikarashi, J. Appl. Phys. 127, 105106 (2020)
- ²¹H. Tews, R. Neumann, A. Hoepfner, and S. Gisdakis, J. Appl. Phys. **67**, 2857 (1990).
- ²²Y. K. Yeo, Y. S. Park, and P. W. Yu, J. Appl. Phys. **50**, 3274 (1979).
- ²³P. Reddy, M. P. Hoffmann, F. Kaess, Z. Bryan, I. Bryan, M. Bobea, A. Klump, J. Tweedie, R. Kirste, S. Mita, M. Gerhold, R. Collazo, and Z. Sitar, J. Appl. Phys. 120, 185704 (2016).
- ²⁴P. Reddy, F. Kaess, J. Tweedie, R. Kirste, S. Mita, R. Collazo, and Z. Sitar, Appl. Phys. Lett. 111, 152101 (2017).
- K. Morizuka, T. Nozu, K. Tsuda, and M. Azuma, Electron. Lett. 22, 315 (1986).
 S. Yamahata and S. Adachi, Appl. Phys. Lett 52, 1493 (1988).